

First-principles molecular dynamics of liquid alkali metals based on the quantal hyper-netted chain theory

Shaw Kambayashi

*Center for promotion of computational science and engineering,
Japan Atomic Energy Research Institute, Tokai, Ibaraki 319-11, Japan*

Junzo Chihara*

*Solid State Physics Laboratory, Japan Atomic Energy Research Institute,
Tokai, Ibaraki 319-11, Japan*

(August 5, 1995)

Abstract

A first-principles molecular dynamics (MD) scheme is presented on the basis of the density-functional (DF) theory with use of the the quantal hyper-netted chain (QHNC) approximation. The DF theory brings about exact expressions for the ion-electron and ion-ion radial distribution functions (RDF's) of an electron-ion mixture as a model of a simple liquid metal. These exact expressions prove that an ion-electron mixture can be treated as a one-component liquid interacting only via a *pairwise* interaction in the evaluation of the ion-ion RDF, and provide a set of integral equations: one is an exact integral equation for the ion-ion RDF and another for an effective ion-ion interaction, which depends on the ion configuration specified by the ion-ion RDF. Hence, after some approximations are introduced, the MD simulation can be per-

*Author to whom correspondence should be addressed.

E-mail: chihara@c3004.tokai.jaeri.go.jp

formed to get the ion-ion RDF using the ion-ion interaction determined so as to be consistent to the ion-ion RDF: the MD simulation and the procedure to determine the effective interaction from the QHNC equation are performed iteratively. This MD simulation coupled with the QHNC equation (QHNC-MD method) for the effective interaction provides a first-principles calculation of structures of simple liquid metal: the ion-ion and electron-ion RDF's, the charge distributions of an ion and a pseudoatom, the effective ion-ion interaction and the ion-ion bridge function are evaluated in a self-consistent manner from the atomic number as the only input.

We have applied this QHNC-MD method to Li, Na, K, Rb and Cs near the melting temperature using upto 16000 particles for the MD simulation. It is found that the convergence of the effective ion-ion interaction is fast enough for practical application to alkali metals; two MD runs are enough for convergence within accuracy of 3 to 4 digits, if the initial effective potential is properly set up. The structure factors, thus obtained, show excellent agreements with experimental data observed by X-ray and/or neutron scattering.

61.25.Mv, 61.20.Gy, 61.20.Ja, 71.50.+t, 31.20.Rx

I. INTRODUCTION

The liquid alkali metals have been studied extensively in both experimental and theoretical sides. They can be easily used to test a theoretical approach as the first step, since they constitute “simple” metals and “simple” liquids: furthermore, there exist many reliable experimental results to be compared. In the standard theory, a liquid metal is treated as a one-component liquid interacting via a binary effective potential, which is determined by the pseudopotential formalism; a pseudopotential is introduced either by first-principles calculations or by adjusting parameters involved in model potentials to some experimental results. In this treatment, the ionic structures are determined independently of the electronic structures in a liquid metal.

It is only recent that a liquid metal is thought of as an electron-ion mixture and the ionic structures are determined in a coupled manner with the electronic structures. One of such approaches is the Car-Parrinello molecular-dynamics (CP-MD) technique [1], where a liquid metal is taken as a binary mixture of ions and electrons. In the CP-MD method, the electron-ion interaction is described by a pseudopotential to produce pseudo-wavefunctions which can be accurately represented by small number of plain waves. The CP-MD method possesses advantage to avoid the difficult task of constructing an effective ion-ion potential required to perform the molecular-dynamics simulation, and afford to provide *ab initio* calculations of metallic systems in principle. However, the most serious problem in this approach is that the number of particles used in the simulations cannot be taken large and a total of time steps performed in the simulations is limited to a small size within the present computational resources. In the present work, we propose another scheme of *first principles* molecular-dynamics simulation based on the density-functional (DF) method applied to the ion-electron mixture; this simulation method can be performed on the large number of particles to last a large size of time steps, since this scheme reduces the electron-ion problem to a usual classical MD coupled with a set of integral equations determining an effective ion-ion interaction: a problem to determine the ion-configuration structure and the

ion-ion interaction in a self-consistent manner.

Previously, we have proposed a set of integral equations for radial distribution functions (RDF's) in an electron-ion mixture on the basis of the DF theory in the quantal hyper-netted (QHNC) approximation [2,3]. In this QHNC formalism, the bare electron-ion interaction $v_{\text{el}}(r)$ and the ionic charge Z_{I} are determined self-consistently by regarding a liquid metal as a mixture of nuclei and electrons [4]. Already, we have applied this approach to liquid metallic hydrogen [2], lithium [5], sodium [6], potassium [7] and aluminum [8] obtaining ion-ion structure factors in excellent agreements with experiments. The QHNC equations are derived from exact expressions for the electron-ion and ion-ion RDF's in an electron-ion mixture: these exact expressions are only formal results derived from the DF theory. A molecular-dynamics scheme to treat an ion-electron mixture can be set up on the basis of these exact relations, which states that the electron-ion mixture can be regarded as a quasi-one component liquid interacting via a *pairwise* interaction in the description of the ion-ion RDF [3] (hereafter, referred to as the QHNC-MD method). Since the QHNC formalism is derived on the electron-ion model where the bound-electrons forming an ion in a liquid metal is assumed to be clearly distinguished from the conduction electrons and the overlap of the core electrons is negligible, the QHNC-MD method is only applicable to simple liquid metals: its application to liquid alkali metals is taken as an ideal test of the QHNC-MD method. Thus, the QHNC-MD method has been shown to yield structure factors of liquid alkali metals in excellent agreement with experiments as the result of a first-principles calculation in the present work.

In Sec. II, we sketch the QHNC formulation: exact expressions for RDF's in an electron-ion mixture are obtained from the DF method [10], and the nucleus-electron model is shown to provide a bare electron-ion interaction, which should be determined self-consistently. The procedure to perform the MD simulation based on the QHNC theory is shown in Sec. III: in the QHNC formulation the effective ion-ion interaction used in the MD simulation depends on the ionic structure specified by the ion-ion RDF. Therefore, in the application of this MD scheme it is important to extrapolate the MD RDF beyond the truncation radius of the

simulation correctly so as to be used in the determination of effective ion-ion interaction; this is exemplified by the method described in Sec. III. Numerical procedure of the QHNC-MD method and the results of its application to alkali liquid metals are described in Sec. IV. The last section is devoted to a discussion, where the advantage/disadvantage of the QHNC-MD method against the CP-MD method is argued also.

II. QUANTAL HYPER-NETTED CHAIN THEORY

A simple liquid metal can be thought of as a binary mixture of ions with a definite ionic charge Z_I and the conduction electrons; the interactions $v_{ij}(r)$ between particles $[i, j = I \text{ or } e]$ are taken as pair-wise. The ions constitute a classical fluid, while the conduction electrons form a quantum fluid. Let us refer to this mixture as the ion-electron model for a liquid metal. Since the ions are regarded as classical particles in the electron-ion model, the ion-ion and electron-ion RDF's become identical with the ion- and electron-density distributions around a fixed ion in the mixture, respectively [3]. Because a fixed ion causes external potentials acting on ions and electrons in the homogeneous mixture, the DF theory can give the exact expressions for the ion- and electron-density distributions, $n_I(r|I)$ and $n_e(r|I)$, in terms of those of noninteracting systems $n_i^0(r)$ under effective external potentials $U_i^{\text{eff}}(r)$ [$i=I, e$]

$$U_i^{\text{eff}}(r) = v_{iI}(r) + \frac{\delta \mathcal{F}_{\text{int}}}{\delta n_i(r|I)} - \mu_i^{\text{int}} \quad (1)$$

with the use of \mathcal{F}_{int} and μ_i^{int} , the interaction part of the intrinsic free-energy and the chemical potential, respectively [9]. As a result, the DF theory provides exact, but formal, expressions for the ion-ion RDF $g_{II}(r)$ and electron-ion RDF $g_{eI}(r)$ as follows:

$$n_0^I g_{II}(r) = n_I(r|I) = n_I^0(r|U_I^{\text{eff}}) \equiv n_0^I \exp[-\beta U_I^{\text{eff}}(r)] , \quad (2)$$

$$n_0^e g_{eI}(r) = n_e(r|I) = n_e^0(r|U_e^{\text{eff}}) \equiv \sum_i \frac{|\psi_i(r)|^2}{\exp[\beta(\varepsilon_i - \mu_0^e)] + 1} , \quad (3)$$

where μ_0^e denotes the chemical potential of a non-interacting electron gas, n_0^I (n_0^e) is the number density of ions (electrons), and $\beta = (k_B T)^{-1}$ the inverse temperature. The electron-

density distribution $n_e^0(r|U)$ is determined by solving the wave equation for an electron under the external potential $U(r)$

$$\left[-(\hbar^2/2m)\nabla^2 + U(r) \right] \psi_i(r) = \varepsilon_i \psi_i(r) . \quad (4)$$

In the similar way to the case of classical binary mixtures, the effective external potentials $U_i^{\text{eff}}(r)$ given by Eq. (1) are written as

$$U_i^{\text{eff}}(r) = v_{i\text{I}}(r) - \Gamma_{i\text{I}}(r)/\beta - B_{i\text{I}}(r)/\beta , \quad (5)$$

$$\Gamma_{i\text{I}}(r) \equiv \sum_l \int C_{il}(|\mathbf{r} - \mathbf{r}'|) n_0^l [g_{l\text{I}}(r) - 1] d\mathbf{r}' , \quad (6)$$

in terms of the direct correlation functions (DCF's) $C_{ij}(r)$ and the bridge functions $B_{i\text{I}}(r)$. Here, the DCF's $C_{ij}(r)$ in the ion-electron mixture are defined within the framework of the DF theory by

$$C_{ij}(|\mathbf{r} - \mathbf{r}'|) \equiv -\beta \frac{\delta^2 \mathcal{F}_{\text{int}}[n_I, n_e]}{\delta n_i(\mathbf{r}) \delta n_j(\mathbf{r}')} \Big|_0 , \quad (7)$$

where the suffix 0 denotes the functional derivative at the uniform densities [9]. Actually the explicit expression for the DCF's are given by the Fourier transform in the matrix form

$$\sqrt{\mathcal{N}} C(k) \sqrt{\mathcal{N}} = (\tilde{\chi}_Q^0)^{-1} - (\tilde{\chi}_Q)^{-1} \quad (8)$$

in terms of the density response functions, $\tilde{\chi}_Q \equiv \| \chi_{ij}(k) \|$ and $\tilde{\chi}_Q^0 \equiv \| \chi^{0i}(Q) \delta_{ij} \|$, of the interacting and noninteracting systems, respectively, with $\mathcal{N} \equiv \| n_0^i \delta_{ij} \|$ [9]. Note here that the density-density response functions $\chi_{iI}(Q)$ concerning ion reduce to the structure factors $S_{iI}(Q)$ and $\chi^{0I}(Q) = 1$, since the ions behave as classical particles [3]. From this definition of the DCF's the Ornstein-Zernike relations are derived for the ion-electron mixture:

$$g_{i\text{I}}(r) = C_{i\text{I}}(r) + \Gamma_{i\text{I}}(r) , \quad (9)$$

$$g_{e\text{I}}(r) = \hat{B} C_{e\text{I}}(r) + \hat{B} \Gamma_{e\text{I}}(r) . \quad (10)$$

Here, \hat{B} denotes an operator defined by

$$\mathcal{F}_Q[\hat{B}^\gamma f(r)] \equiv (\chi_Q^0)^\gamma \mathcal{F}_Q[f(r)] = (\chi_Q^0)^\gamma \int \exp[i\mathbf{Q} \cdot \mathbf{r}] f(r) d\mathbf{r} , \quad (11)$$

for an arbitrary real number γ , and represents a quantum-effect of the electron through the density response function χ_Q^0 of the non-interacting electron gas.

A set of integral equations (2) and (3) are exact but formal expressions, as well as all other equations in the above. However, the ionic charge Z_I and the electron-ion interaction $v_{ei}(r)$ must be given beforehand, when we apply these formula to a liquid metal as an ion-electron mixture. In order to determine these quantities from first principle, a liquid metal must be treated more fundamentally as a mixture of nuclei and electrons (the nucleus-electron model), where all interactions between particles are known as pure Coulombic. In this model, input data in dealing with a liquid metal is only the atomic number Z_A to specify the material. For this purpose, let us consider a liquid metal as a mixture of N_I nuclei and $Z_A N_I$ electrons, and solve the problem to determine the electron-density distribution around a nucleus fixed at the origin in this mixture. Since a fixed nucleus causes an external potential $U(r) = -Z_A e^2/r$ for this mixture to produce an inhomogeneous system, the DF theory can be applied to this problem. It should be noticed that DF theory contains some arbitrariness in the choice of a reference system to describe the system [9]. We can get a simple description of the nucleus-electron mixture if the reference system is chosen to be a mixture consisting of $N_I - 1$ noninteracting ions and $Z_I(N_I - 1) + Z_A$ noninteracting electrons: here, each ion is assumed to have Z_B bound-electrons with a charge distribution $\rho_b(r)$ around it and an ionic charge $Z_I \equiv Z_A - Z_B$. With use of this reference system, the DF theory can provide an effective external potential $v_{eN}^{\text{eff}}(r)$ for electrons around the fixed nucleus. Then, the electron-density distribution $n_e(r|N)$ around the fixed nucleus is obtained by solving the wave equation for $v_{eN}^{\text{eff}}(r)$ in the sum of the bound- and free-electron parts:

$$n_e(r|N) = n_e^{\text{ob}}(r|v_{eN}^{\text{eff}}) = n_e^{\text{b}}(r|N) + n_e^{\text{f}}(r|N) . \quad (12)$$

Hence, the bound-electron distribution $n_e^{\text{b}}(r|N)$ thus determined constitutes the definition of the “ion” in the electron-ion model. Furthermore, this bound-electron distribution $n_e^{\text{b}}(r|N)$ should be taken identical with the electron distribution $\rho_b(r)$ of an ion in the reference system, since the ion formed around the central nucleus is necessary to be the same structure

as any ion in the system. Thus, we obtain a self-consistent condition to determine the distribution $\rho_b(r)$ in the premise:

$$\rho_b(r) = n_e^b(r|N) \equiv n_e^b(r) \quad (13)$$

with the bound-electron number $Z_B = \int \rho_b(r) d\mathbf{r}$. On the other hand, the free-electron part $n_e^f(r|N)$ in Eq. (12) is taken as the electron-ion RDF $n_0^e g_{ei}(r)$ of the electron-ion mixture with the free-electron density $n_0^e = Z_I n_0^I$, and the nucleus-nucleus RDF becomes the ion-ion RDF $g_{II}(r)$.

With use of this reference system, we can obtain a tractable expression of $v_{eN}^{\text{eff}}(r)$ for the wave equation to determine $n_e(r|N)$ by introducing some approximations to the exchange-correlation term involved in it [4]:

$$v_{eN}^{\text{eff}}(r) = \tilde{v}_{eI}(r) - \frac{1}{\beta} \sum_l \int C_{el}(|\mathbf{r} - \mathbf{r}'|) n_0^l [g_{Il}(r') - 1] d\mathbf{r}' , \quad (14)$$

where $\mu_{XC}(n)$ is the exchange-correlation potential in the local-density approximation (LDA). Note that this expression is equal to Eq. (5) without the electron-ion bridge functions $B_{eI}(r)$ except that the bare electron-ion interaction is explicitly given by

$$\tilde{v}_{eI}(r) \equiv -\frac{Z_A e^2}{r} + \int v_{ee}(|\mathbf{r} - \mathbf{r}'|) n_e^b(r') d\mathbf{r}' + \mu_{XC}(n_e^b(r) + n_0^e) - \mu_{XC}(n_0^e) . \quad (15)$$

In this way, the treatment of a liquid metal as a nucleus-ion mixture is shown to provide the ion-electron model, where the bare electron-ion interaction $\tilde{v}_{eI}(r)$ and the ionic structure $\rho_b(r)$ can be determined in a self-consistent manner.

With the help of the result from the nucleus-electron model, we can derive a closed set of integral equations for the ion-electron mixture, if we introduce the following approximations: (A) the electron-ion bridge function in Eq. (21) is neglected: $B_{eI}(r) \simeq 0$, (B) the electron-electron DCF $C_{ee}(r)$ is approximated [3] as

$$C_{ee}(Q) = -\beta v_{ee}(Q) [1 - G^{\text{jell}}(Q)] . \quad (16)$$

using the local-field correction (LFC) $G^{\text{jell}}(Q)$ of the jellium model for an electron gas, (C) the bare ion-ion potential $v_{II}(r)$ is taken as pure Coulombic, i.e., $v_{II}(r) = (Z_I e)^2 / r$, and

(D) the bare electron-ion potential is given by $v_{\text{el}}(r) = \tilde{v}_{\text{el}}(r)$ of Eq. (15). We have called this set of equations the quantal hyper-netted chain equations because of the approximation $B_{\text{el}}(r) \simeq 0$ in Eq. (5).

III. MOLECULAR DYNAMICS SIMULATION BASED ON QUANTAL HYPER-NETTED CHAIN THEORY

It is important to realize that the electron-ion model leads to the neutral-fluid model, where the ionic behavior of a liquid metal is taken to be the same as a neutral one-component fluid interacting via a binary effective interaction in treating the ion-ion RDF. This neutral-fluid model is derived from the electron-ion model, when an effective ion-ion potential is defined in such a way that the RDF of a one-component fluid should become identical with $g_{\text{II}}(r)$ of the electron-ion mixture:

$$g(r) \equiv \exp[-\beta v_{\text{eff}}(r) + \Gamma(r) + B(r)] = g_{\text{II}}(r) , \quad (17)$$

with use of the Ornstein-Zernike relation for a neutral one-component fluid

$$g(r) - 1 = C(r) + \Gamma(r) . \quad (18)$$

In the above, the DCF for the one-component fluid is defined by $n_0^{\text{I}}C(Q) \equiv 1 - S_{\text{II}}(Q)^{-1}$ and $\Gamma(r) \equiv \int C(|\mathbf{r} - \mathbf{r}'|)n_0^{\text{I}}[g(r') - 1]d\mathbf{r}'$.

Thus, we can write the explicit expression for the effective ion-ion potential of a liquid metal in the neutral-fluid model as

$$\beta v_{\text{eff}}(Q) \equiv \beta v_{\text{II}}(Q) - \frac{|C_{\text{el}}(Q)|^2 n_0^{\text{e}} \chi_Q^0}{1 - n_0^{\text{e}} C_{\text{ee}}(Q) \chi_Q^0} , \quad (19)$$

by taking the bridge function $B(r)$ to be $B_{\text{II}}(r)$ of the electron-ion mixture. Equation (19) can be interpreted within the scope of the standard pseudopotential theory by regarding $C_{\text{el}}(r)$ as the pseudopotential $w_b(Q) = -C_{\text{el}}(Q)/\beta$. In this way, the ion-electron model is reduced exactly to the neutral-fluid model with a *binary* effective interaction Eq. (19), in which the many-body forces are taken into account in the form of the linear response

expression (19), since the nonlinear effect in the electron screening is involved in terms of the electron-ion DCF, which plays the role of a nonlinear pseudopotential.

By noting the above relations (17)–(19), the exact expressions (2)–(10) for the electron-ion model can be transformed into a set of integral equations: one is the integral equation for a one-component fluid with the effective ion-ion potential $v_{\text{eff}}(r)$

$$C(r) = \exp[-\beta v_{\text{eff}}(r) + \Gamma(r) + B(r)] - 1 - \Gamma(r) , \quad (20)$$

and the other an equation for the effective ion-ion interaction $v_{\text{eff}}(r)$, that is expressed in the form of an integral equation for the electron-ion DCF $C_{\text{el}}(r)$:

$$\hat{B}C_{\text{el}}(r) = n_{\text{e}}^0(r[v_{\text{el}} - \Gamma_{\text{el}}/\beta - B_{\text{el}}/\beta]/n_0^{\text{e}} - 1 - \hat{B}\Gamma_{\text{el}}(r) , \quad (21)$$

since the effective interaction $v_{\text{eff}}(r)$ is given in terms of $C_{\text{el}}(r)$ by Eq. (19). In contrast with the usual effective potential in the pseudopotential theory, the effective potential (19) depends on the ion configuration represented by the ion-ion RDF $g_{\text{II}}(r)$ through the term: $\Gamma_{\text{el}}(r) \equiv \sum_l \int C_{\text{el}}(|\mathbf{r} - \mathbf{r}'|) n_0^l [g_{\text{II}}(r) - 1] d\mathbf{r}'$ in Eq. (21).

Under the assumptions (A)–(D) mentioned before, the QHNC equations (20) and (21) enables us to perform an *ab initio* molecular-dynamics (MD) simulation which requires only the atomic number Z_{A} and thermodynamic states as input parameter, in principle. The first estimation for $v_{\text{eff}}(r)$ can be obtained with use of $C_{\text{el}}(r)$ evaluated by Eq. (21) with an initial guess for $g_{\text{II}}(r)$. Next, an integral equation (20) for a one-component fluid can be solved by performing the classical MD simulation for this $v_{\text{eff}}(r)$ to produce new ion-ion RDF $g_{\text{II}}(r)$; this is used again in Eq. (21) to determine a new estimation for $v_{\text{eff}}(r)$. This process will be continued until convergence of the effective ion-ion potential is achieved (we refer to this procedure as the QHNC-MD method). However, such a straight-forward repetition of the MD simulation to solve the QHNC equations is not practical in the viewpoint of the computational cost. Since the dependence of the effective ion-ion potential $v_{\text{eff}}(r)$ on the ionic configuration is rather weak in a simple metal as we have shown in [8], we can adopt an approximate theory for $B(r)$ in Eq. (20) to get an initial $v_{\text{eff}}(r)$ for the QHNC-MD method.

For this purpose, we take the variational modified HNC (VMHNC) equation proposed by Rosenfeld [11], in which the bridge function is approximated by $B_{PY}(r; \eta)$ of the Percus-Yevick equation for hard-spheres of diameter σ with the packing fraction $\eta = \pi n_0^I \sigma^3 / 6$. In the VMHNC equation, the adjustable parameter η is determined by the following condition:

$$\frac{1}{2} n_0^I \int [g(r) - g_{PY}(r; \eta)] \frac{\partial B_{PY}(r; \eta)}{\partial \eta} d\mathbf{r} + \frac{2\eta^2}{(1 - \eta)^3} = 0, \quad (22)$$

where $g_{PY}(r; \eta)$ is the RDF for the hard-sphere fluid with the Percus-Yevick equation. Thus, in a similar way to the QHNC-MD method, the integral equation (20) in the VMHNC approximation is solved in a coupled manner with Eq. (21) producing new effective ion-ion interaction [referred to as the QHNC-VM method]. Furthermore, an initial potential $v_{\text{eff}}(r)$ to this QHNC-VM method can be obtained by approximating $g_{II}(r)$ in Eq. (21) by the step function $\theta(r - a)$ with the ion-sphere radius $a = (4\pi n_0^I / 3)^{-1/3}$. When this final $v_{\text{eff}}(r)$ from the QHNC-VM method is used as an input to the QHNC-MD method, the convergent result can be obtained by a few repetition of MD simulation. Finally our procedure to solve the QHNC equation with the MD simulation (the QHNC-MD method) is summarized as the flow chart shown in Figure 1. For an initial potential $v_{\text{eff}}(r)$ given by approximation $g_{II}(r) = \theta(r - a)$, the QHNC-VM method in the *preparation phase* yields a good initial guess for the QHNC-MD method. Then the MD simulation is repeatedly performed to achieve convergence of $v_{\text{eff}}(r)$ in the *refinement phase*.

There are two important points to be noticed regarding the MD simulation when applied to the QHNC-MD method. One is that the computer simulation provides the RDF $g(r)$ only within the half of the side length L of the simulation cell. This causes an unavoidable truncation error in calculation of the Fourier transform $\mathcal{F}_Q[g(r) - 1]$ to be used in the evaluation of Eqs. (19) and (21). The second point is that the MD simulation is performed inevitably on a truncated potential for a liquid metal whose effective ion-ion potential is accompanied by a long-ranged oscillatory tail: the computer simulation may yield different RDF's depending on the cutoff radius R_c of the potential. Recently we have proposed a precise procedure [10] to improve these two defects at the same time and to get the RDF in

the whole range of distance for the full potential $v_{\text{eff}}(r)$. This method can be applied even to the *small-size* simulation result for the truncated potential $u_c(r)$:

$$u_c(r) \equiv \begin{cases} v_{\text{eff}}(r) - v_{\text{eff}}(R_c) & \text{for } r < R_c \\ 0 & \text{for } r \geq R_c \end{cases}. \quad (23)$$

As the first step of this procedure, we extract the bridge function from the raw MD RDF data. For this purpose, we extend the the raw RDF data of the MD simulation $g_{\text{MD}}(r)$, by solving an integral equation

$$g(r) \equiv \begin{cases} g_{\text{MD}}(r) & \text{for } r < R \\ \exp[-\beta u_c(r) + \Gamma(r)] & \text{for } r \geq R \end{cases}, \quad (24)$$

coupled with the Ornstein-Zernike relation, where R is the extrapolating distance ($R < L/2$). At this stage, in order to obtain a reliable bridge function, it is essential to take R as short as about 3 to 4 interatomic spacings or simply as $R = R_c$ [10] and to discard the RDF data outside the distance R so as to reduce the statistical noise contained in the raw RDF data. Using the extended $g(r)$, the bridge function $B_{\text{MD}}(r)$ can be extracted for distances where $g_{\text{MD}}(r) \neq 0$ by

$$B_{\text{MD}}(r) \equiv \begin{cases} \beta u_c(r) + \ln[g_{\text{MD}}(r)] - \Gamma(r) & \text{for } r < R \\ 0 & \text{for } r \geq R \end{cases}. \quad (25)$$

At the second step to get the RDF for the full potential $v_{\text{eff}}(r)$, we solve the integral equation (20) for the full potential with use of this $B_{\text{MD}}(r)$ as an approximation to that of the full potential: this can be justified by the fact that the bridge function is not sensitive to the long-range part of the potential and becomes very weak for long-range distance [10].

IV. APPLICATION TO LIQUID ALKALI METALS

A. Numerical procedure of QHNC-MD method

Liquid alkali metals constitute “simple” metals in the sense that the bound electrons forming an ion are clearly distinguished from the conduction electrons and the overlap

of the core electrons are negligible; the approximations (A)–(D) used in the QHNC-MD method become quite good ones for these metals. Therefore, we have applied the QHNC-MD method for five liquid alkali metals (Li, Na, K, Rb, and Cs) near the melting point using the parameters specified in Table I; the temperature and density have been chosen to be compared with experimental data in [12–17]. Here, the temperature and density of alkali liquids are specified by two dimensionless parameters: the plasma parameter $\Gamma = \beta e^2/a$ and $r_s = a/a_B$ in units of the Bohr radius a_B , with the average ion-sphere radius a .

In our application of the QHNC-MD simulation to the alkali liquids, the local-field correction of the jellium model in Eq. (16) is chosen to be that proposed by Geldart and Vosko [22], since it has a simple structure and gives a good approximation. In Eq. (15), the expression given by Gunnarsson and Lundqvist [23] is adopted as the LDA for the exchange-correlation potential $\mu_{XC}(n)$.

After the preparation of initial effective potential by the QHNC-VM method, two iterations in the refinement phase of the QHNC-MD method (Figure 1) are sufficient to obtain a convergent solution for alkali liquid metals; 16,000 particles have been used in the first MD run (Run-1) and 4,000 particles for the second MD run (Run-2). The MD simulation has been performed over 50,000 time steps for Run-1 and 100,000 time steps for Run-2 with the cubic periodic boundary conditions; the temperature of the system is kept constant by the isokinetic constraint [18]. The equations of motion are integrated by a fifth order differential algorithm [19] with the time increment $\Delta t = 0.0025 n_0^{1-1/3} (m_i \beta)$ with the mass of an ion m_i ; the corresponding real time is shown in Table I. In each MD simulation of Run-1 and Run-2 for iterations, the effective potential is cut at the radius R_c located at the node of the Friedel oscillation of $v_{\text{eff}}(r)$ as shown in Table I. All MD simulations have been carried out on a vector-parallel processor Monte-4 [20] at Japan Atomic Energy Research Institute. The computational time required for 10,000 steps is about 30 to 50 hours for 16,000 particles including the sampling of the RDF.

The integral equation (24) has been solved by an iterative procedure introduced by Ng [21] to extend the raw MD data $g_{\text{MD}}(r)$ to the whole r range: the extending distance R

in this procedure (24) is taken to be R_c for the whole cases. The number of grid points and step size used in numerical integrations are 1024 points and $\Delta r = 0.025a$, respectively. Using $C(r)$ obtained by the HNC equation as an initial input function, it takes about 10,000 iterations to achieve convergence.

In order to examine both numerical and computational efficiency of the QHNC-MD method, we have tested the convergence of the RDF by evaluating following consistency measure for $g(r)$:

$$\Delta g_i(r) \equiv g_i(r) - g_{i-1}(r) , \quad (26)$$

$$|\Delta g_i| \equiv \left(\frac{4\pi n_0^I}{3} \int_0^\infty |\Delta g_i(r)|^2 r^2 dr \right)^{1/2} . \quad (27)$$

Here $g_i(r)$ is $g_{\text{II}}(r)$ obtained by the i -th MD simulation and $g_0(r)$ is that obtained by the final step of the preparation phase. Figure 2 shows the consistency measure (26) of the present QHNC-MD simulation for the case of liquid Li, yielding the values $|\Delta g_1| = 1.53 \times 10^{-1}$ and $|\Delta g_2| = 5.92 \times 10^{-3}$. It is easily seen that the convergence of $g_{\text{II}}(r)$ is very fast; the difference of $g_{\text{II}}(r)$ between Run-1 and Run-2 is situated almost within the statistical error of the sampling of the RDF in the MD simulation: this means accuracy of about 3 to 4 digits is already achieved in the QHNC-MD calculation of Run-1. In a consistent way to the convergence of the RDF, a good convergence of the effective ion-ion potential $v_{\text{eff}}(r)$ is achieved in Run-1. Similar to the case of liquid Li, a good convergence of $g_{\text{II}}(r)$ and $v_{\text{eff}}(r)$ is also achieved for other liquid metals. It should be noted that the preparation phase of the QHNC-MD method largely enhances the convergence of $v_{\text{eff}}(r)$.

Concerning the treatment of the raw MD data for the ion-ion RDF, it should be emphasized that the extension procedure [10] to obtain the RDF for the full potential applied to the raw MD data is indispensable for the present calculation. This situation is illustrated in Fig. 3, where the truncation error in $g_{\text{II}}(r)$ due to the use of the cutoff potential in the MD simulation is so large that the convergence of the QHNC-MD method will not be attained with the raw RDF data. In addition, the extended RDF for the full potential is almost identical with the result of VMHNC equation for the same potential (Figure 3) for $r \gtrsim 5a$,

i.e., after the third peak of RDF. This suggests that the long ranged Friedel oscillation of $v_{\text{eff}}(r)$ typically seen for liquid metals is essential for the detailed structure of the RDF at long distances, and it is necessary to include the information of the long-range part of $v_{\text{eff}}(r)$ into $g_{\text{II}}(r)$ in order to obtain a self-consistent solution of the effective ion-ion potential by the QHNC-MD calculation.

It is concluded that the convergence of the present QHNC-MD simulation is well attained from both numerical and computational points of view, helped by a good initial estimation from the VMHNC equation in the preparation phase; the extension procedure to obtain the full-range RDF for the uncut effective potential is also necessary to get the convergence.

B. Ion-ion and electron-ion radial distribution functions

Following the procedure mentioned above, we obtain the effective interatomic interaction, the ion-ion and electron-ion RDF's, the charge distribution $\rho(r)$ of neutral pseudoatom, the bound electron distribution $n_{\text{b}}(r)$ forming an ion and the bridge functions for liquid alkali metals in a self-consistent way from the atomic number as the only input. In the first place, we show structure factors, the Fourier transform of the ion-ion RDF's. It is important for a detail comparison with experiment to use the MD RDF corrected for a full potential and extrapolated to whole range of distance in its Fourier transform.

Figure 4 exhibits the structure factors for liquid Li calculated by the QHNC-MD simulation in comparison with the experimental result [12]. It is clearly seen that the present result is in excellent agreement with the experiment, improving the detailed structure of $S_{\text{II}}(Q)$ near its second peak compared with the result of the VMHNC equation (the final result of the preparation phase). This improvement on $S_{\text{II}}(Q)$ by the refinement phase essentially relies on the detailed oscillatory behavior of the bridge function extracted from the raw RDF of the MD simulation. The discrepancy in the bridge function between the MD simulation and VMHNC equation gives no serious effects on the first peak of the RDF. But details of the RDF for $2a \lesssim r \lesssim 5a$ are rather sensitive to the oscillation of $B(r)$ in a similar way as

discussed in [10]. Therefore the use of the extracted bridge function $B_{\text{MD}}(r)$ to determine the corrected RDF is important in order to guarantee the correct behavior of the structure factor by the Fourier transform. The structure factors calculated for Na and K are shown in Fig. 5 in comparison with the neutron and X-ray experiments [13,14]. The QHNC-MD structure factor of Na is in excellent agreement with the X-ray result (full circles) showing a small deviation from the neutron data (circles) at the first peak, while the curves of the QHNC-MD structure factor for K lies between the neutron (circles) and X-ray (full circles) experimental results. Also, the structure factors from the QHNC-MD method for Rb and Cs are compared with the neutron and X-ray experiments [15–17] in Fig. 6. The first peak of Rb structure factor observed by neutron experiment (full circles) [15] is shifted a little to large Q side compared with that observed the X-ray experiment (circles) [17]; the QHNC-MD result has the same first-peak position to the X-ray data with a little different height and shows overall agreement with the neutron observation. On the other hand, the QHNC-MD structure factor of Cs becomes higher in the first-peak than the experiment [13] and shows a small deviation in the phase of oscillation of structure factor for the large Q region compared with experiment. In our treatment, we solve the Schrödinger equation to obtain the bound-electron distribution and electron-ion RDF; the relativistic effect is not taken into account. In the case of Cs, the relativistic effect may contribute to the calculation of the structure factor, since its atomic number $Z_A = 55$ is rather large; there is a possibility that this effect may be ascribed to this small discrepancy between the calculated and experimental results in Cs structure factor. In the same way as shown in the Li structure factor, the QHNC-VM structure factors deviate from the QHNC-MD results near the their second peak for Na, K, Rb and Cs as seen Figs. 5 and 6. This second-peak difference between the QHNC-MD and QHNC-VM structure factors brings about a distinct difference in the RDF's obtained from their Fourier transform, as can be seen from an example of Na shown in Fig. 7. Thus, the RDF from the VMHNC equation is found not so exact as to compare with details of experimental results for alkali liquids; the QHNC-MD method is shown to produce reliable results for all alkali liquids.

Next, we proceed to discuss the electronic structure around ion. The electron-ion RDF's from the QHNC-MD method are shown in Fig. 8 for the case of Rb at temperature 313 K together with the ion-ion RDF. The electron-ion structure factor $S_{\text{el}}(Q)$ is represented in the form [2]:

$$S_{\text{el}}(Q) = \frac{\rho(Q)}{\sqrt{Z_I}} S_{\text{II}}(Q), \quad (28)$$

in terms of the ion-ion structure factor and the charge distribution of the pseudoatom:

$$\rho(Q) \equiv \frac{n_0^e C_{\text{el}}(Q) \chi_Q^0}{1 - n_0^e C_{\text{ee}}(Q) \chi_Q^0}. \quad (29)$$

With the help of the above equations, the pseudopotential method using the Ashcroft model potential can evaluate the electron-ion RDF by inserting it in (29) instead of $-C_{\text{el}}(r)/\beta$; its result using the empty core radius 1.27\AA has no inner-core structure near the origin as is expected. In the QHNC-MD method, we need not introduce any pseudization in treating the core region. Therefore, the electron-ion RDF $g_{\text{el}}(r)$ exhibits the inner-core structure similar to a free-atom as is shown in Fig. 8 in contrast with result of the pseudopotential method (full circles). It is interesting to note that the electron-ion RDF has an oscillation with an inverse phase to that of the ion-ion RDF, since the electrons are pushed away by an ion as a whole in the core region. The charge distribution $\rho(r)$ of the pseudoatom in a liquid Rb has a similar structure to the distribution $\rho_{5s}(r)$ of the $5s$ -electrons in the free-atom; therefore, the total electron-density distribution $n_b(r) + \rho(r)$ is almost same to that of a free atom as was indicated by Ziman. Also, note that the positions of the dips in the electron-ion RDF are coincident with those appeared in the $5s$ -electron charge distribution $\rho_{5s}(r)$ in a free-atom; these dips in the electron-ion RDF reflect the inner structure of an ion in a metal. The electron-ion RDF's of liquid alkali metals (Li, Na, K, Rb and Cs) are shown in Fig. 10, where the inner-core structure is omitted near the origin in each curve. The dip in the electron-ion RDF becomes shallower and is shifted to the right side indicating the growth of the core size, as the atomic number increases from Na to Cs: the curve of Li shows an exception to this tendency.

When the electron-ion RDF is determined by solving the wave equation for the self-consistent potential $v_{\text{el}}^{\text{eff}}(r)$, we obtain from Eq. (21) the electron-ion DCF $C_{\text{el}}(r)$, which yields an effective ion-ion potential $v_{\text{eff}}(r)$ of Eq. (19). Corresponding to each curves of $g_{\text{el}}(r)$ in Fig. 10, the effective ion-ion potential $v_{\text{eff}}(r)$ is determined for each element as shown in Fig. 11. It should be emphasized that there is no units for scaling lengths and energies to effective ion-ion potentials determined by the QHNC-MD method in contrast with those obtained by using the Ashcroft model potential [24]. Similarly, no scaling features are found in the effective ion-ion potential obtained by the Dagens-Rasolt-Taylor method [25], which can be thought of as an approximation to the QHNC formulation in the sense that the ion-ion RDF is there replaced by the spherical vacancy in Eq. (14) [26]. Nevertheless, it is shown that for liquid alkali metals near the melting point the ion-ion RDF's from the QHNC-MD method can be scaled almost into one curve by taking the average ion radius a in the units of length as indicated in Fig. 12 except Cs.

As the summarization of this section, we conclude that the present application of the QHNC-MD method to liquid alkali metals provides the ionic structures in excellent agreement with the experiments within the computational capacity available at present, enabling to handle a relatively large system size in the MD simulation in contrast with the usual *ab initio* simulation for the electron-ion mixture. So as to be consistent with the ionic structure specified by the ion-ion RDF, the QHNC-MD method is shown to give the electron-ion RDF $g_{\text{el}}(r)$, the charge distribution $\rho(r)$ of a pseudoatom and the density distribution $n_{\text{b}}(r)$ of the bound electrons forming an ion in a liquid metal at the same time; alternatively this electronic structure produces the ion-ion potential $v_{\text{eff}}(r)$ used for the MD simulation.

V. DISCUSSION

We have shown that the QHNC-MD formulation provides a very precise description of simple liquid metals at any state from the atomic number Z_{A} as the only input: this method is proven to yield a first-principles calculation. Our previous calculations with the VMHNC

equation, which has been used for input to the QHNC-MD method, generated the structure factors with a small but systematic deviation from experiments near the second peak. Now our QHNC-MD method is shown to correct this deviation and to yield results in excellent agreement with experiments in the whole range of wavenumber Q . Even in alkali metals, there is no scaling unit of lengths and energies for the effective ion-ion potentials $v_{\text{eff}}(r)$ determined from the QHNC-MD method; each potential is different from other and reflects a difference in the bound-electron structure of an ion in each metal. The situation is different in the case of the effective potential calculated by use of the Ashcroft pseudopotential, which leads to give almost single potential curve for all alkali liquids if scaled with the proper unit [24]. However, it is interesting to note that the ion-ion RDF's can be scaled by the unit of a , the average ion-sphere radius, which enables plot the results in almost single curve for alkali liquids (Li, Na, K, Rb) near the melting point except the case of Cs. This fact was already found in the experimental results for the structure factors [13].

In our QHNC-MD formulation, the exchange-correlation effect expressed by the LFC $G(Q)$ and the LDA $\mu_{\text{XC}}(n)$ are introduced from outside the framework of our formulation: those of the jellium model, where the ion distribution is replaced by the positive uniform background. The jellium model gives a good description for the electrons in alkali metals; the present success of the QHNC-MD method depends on this fact. In addition, the structure factors of alkali metals calculated by this method are almost independent of what kind of LFC to choose. However, it should be noted that the LFC in the QHNC formulation should depend on the ion configuration precisely, since it is defined for the electron-electron DCF in the electron-ion mixture.

To compare the MD structure factors with experiments in detail, it is important to extrapolate the MD RDF to large distances and to correct errors caused by the cut effective ion-ion potential used in the MD simulation. Our extrapolation method [10] is shown very efficient in dealing with the raw MD data for a liquid metal with ion-ion potential accompanied by a long-range Friedel oscillation; this extrapolation method is indispensable to obtain a convergent solution in the QHNC-MD method. In order to obtain so reliable bridge func-

tion for the extrapolation of the MD RDF, it is necessary to get a reasonable statistical accuracy for evaluation of the RDF; for this purpose, the MD simulation must be performed for at least several thousand particles taking about 10^{10} to 10^{11} samples [10].

The Car-Parrinello MD (CP-MD) method is based on the same ground to the QHNC-MD method: the electron-ion mixture model for liquid metals and the jellium model for electrons, which are treated by the DF theory. Also, the bare ion-ion interaction is taken as a pure Coulombic in both treatment. However, in the CP-MD method, the bare electron-ion interaction is approximated by a pseudopotential, which is introduced from outside of the CP-MD formulation; this fact makes a contrast with our QHNC-MD method where it is obtained self-consistently within the framework of the QHNC formulation and no pseudization is necessary in treating the core region. As a consequence, the electron-ion RDF extracted from the CP-MD result does not have an inner core structure. It should be emphasized that in the QHNC formulation the inner electronic structure around a fixed nucleus, such as the electron-ion RDF in the core region and the bound-electron distribution $n_b(r)$ of an ion in a liquid metal, is determined to be consistent with the outer structure, that is, with the surrounding ion and electron configurations. Therefore, the QHNC-MD method can be applied to a high density plasma, where a usual pseudopotential can not be constructed due to the fact the atomic structure in a highly compressed plasma state is quite different from that in the vacuum. While in the CP-MD treatment the electron distribution is determined for the multi-ion configuration and the ions are considered to be interacting via many-body forces, our approach deals with the one-center problem to determine the electron and ion distributions around a fixed ion in a liquid metal. As this connection, it should be kept in mind that the electron-ion mixture can be exactly taken as a quasi one-component system interacting only via a *pairwise* interaction in the evaluation of the ion-ion RDF for simple liquid metals.

The advantage of the present method against the CP-MD method based on the usual pseudopotential theory can be summarized as follows: (1) The present procedure is capable to handle a large system size ($\sim 10^3$ to 10^4 particles) in the MD simulation within

the computational resources available at present, helped by the good initial guess with the VMHNC approximation for solving the QHNC equation. (2) In the QHNC-MD method, the many-body forces and nonlinear effect in the electron screening are taken into account automatically in the form of a pairwise interaction in such a way that the nonlinear pseudopotential is constructed in terms of $C_{\text{el}}(r)$. (3) By setting up an additional integral equation for $C_{\text{ee}}(r)$, our method can treat the case where the jellium model for the electrons in a metal breaks down, that is, where the exchange-correlation effect begins to depend on the ion configuration [2]. Therefore, (4) our method is applicable to high density plasmas where the ionic structure becomes significantly so different from a free atom due to high compression that the usual pseudopotential theory cannot be applied.

The QHNC-MD method is developed on the base of the ion-electron model, where the bound electrons are assumed to be clearly distinguished from the conduction electrons and the ions are so rigid and so small that the ion-ion bare interaction is taken as a pure Coulombic $v_{\text{II}}(r) = (Z_{\text{I}}e)^2/r$. Therefore, our method is applicable only to a simple metallic system. In a transition metal, for example, an “ion” cannot be clearly defined since the bound electrons are not distinct from the conduction electron, and the overlap of “ions” is significant: many-body interactions becomes important. Our method cannot be applied to such a case. While the CP-MD method treat electrons in the multi-center problem, our method treat them as the single-center problem to determine the density distribution around an fixed ion in a liquid metal. Thus, our method cannot describe states of the electrons in a multi-center configuration, such as the density of states. Moreover, it should be noticed that an orbital of an ion determined by the QHNC-MD simulation may be taken as an average orbital in some sense compared with that determined the CP-MD simulation: there, many-body forces are changing at every time-step, while the binary ion-ion interaction remains constant at every time-step in the QHNC-MD simulation. Already, we have proposed a method to treat non-simple metals [3]; the RDF’s, the ionic charge and the muffin-tin potential are determined by solving a single-center problem with a bare ion-ion interaction as an input, while the density of states, the bare ion-ion interaction and the thermodynamic

properties are to be obtained as results of the multi-center problem with use of output from the single-center problem.

The CP-MD method can produce the electron-ion RDF and the electron-ion structure $S_{\text{ei}}(Q)$ is obtained from its Fourier transform. Thus, the charge distribution $\rho(Q)$ of a neutral pseudoatom can be calculated from Eq. (29) even in the CP-MD simulation, since the relation (28) between $\rho(Q)$ and $S_{\text{ei}}(Q)$ is exact if a liquid metal can be treated as a ion-electron mixture. Also, the electron-ion DCF $C_{\text{ei}}(Q)$ is determined from Eq. (29) to give an effective ion-ion interaction $v_{\text{eff}}(r)$ from Eq. (19); these quantities must be consistent to the ion-ion structure factor $S_{\text{II}}(Q)$, if the LFC $G(Q)$ in the electron-electron DCF $C_{\text{ee}}(r)$ is chosen exact one in the electron-ion mixture. In this connection, there is a point to notice regarding the CP-MD method that the exchange-correlation effect of the valence electrons is treated by the LDA approximation: the LFC $G(Q)$ does not appear in the CP-MD method. This consistency test in the CP-MD method can be exemplified by applying it to liquid alkali metals, which are typical examples of the electron-ion model. At the same time, these quantities in the CP-MD method can be compared with the results of the QHNC-MD method, both methods providing first principles calculations.

ACKNOWLEDGMENTS

We would like to thank Center of promotion of computational science and engineering, Japan Atomic Energy Research Institute for permitting us to use a plenty amount of computational resources on the dedicated vector-parallel processor Monte-4.

It is a sad duty to inform the scientific community that Dr. Shaw Kambayashi died on April 3, 1995 following a car accident just after his thirtieth birthday.

REFERENCES

- [1] R. Car and M. Parrinello, *Phys. Rev. Lett.* **55**, 2471 (1985).
- [2] J. Chihara, *Phys. Rev. A* **33**, 2575 (1986).
- [3] J. Chihara, *J. Phys.: Condens. Matter* **3**, 8715 (1991); J. Chihara and M. Ishitobi, *Molecular Simulation* **12**, 187 (1994).
- [4] J. Chihara, *J. Phys. C: Solid State Phys.* **18**, 3103 (1985).
- [5] J. Chihara, *Phys. Rev. A* **40**, 4507 (1989).
- [6] M. Ishitobi and J. Chihara, *J. Phys.: Condens. Matter* **4**, 3679 (1992).
- [7] M. Ishitobi and J. Chihara, *J. Phys.: Condens. Matter* **5**, 4315 (1993).
- [8] J. Chihara and S. Kambayashi, *J. Phys.: Condens. Matter*, **6** 10221 (1994).
- [9] J. Chihara, *J. Phys. C: Solid State Phys.*, **17** 1633 (1984).
- [10] S. Kambayashi and J. Chihara, *Phys. Rev. E* **50**, 1317 (1994);
- [11] Y. Rosenfeld, *J. Stat. Phys.* **42**, 437 (1986).
- [12] H. Olbrich, H. Ruppertsberg and S. Steeb, *Z. Naturforsch.* **38A**, 1328 (1983), where numerical data for $S_{\Pi}(Q)$ is taken from [16],
- [13] M.J. Huijben and W. van der Lugt, *Acta Cryst. A* **35**, 431 (1979), where numerical data of $S_{\Pi}(Q)$ is taken from [16].
- [14] A.J. Greenfield, J. Wellendorf and N. Wiser, *Phys. Rev. A* **4**, 1607 (1971).
- [15] J. R. D. Copley and S. W. Lovesey, *Int. Phys. Conf. Ser.* **30**, 575 (1979), where numerical data of $S_{\Pi}(Q)$ is taken from [16].
- [16] W. van der Lugt and B.P. Alblas, “Structure factor of liquid alkali metals”, in *Handbook of Thermodynamics and Transport Properties of Alkali Metals*, R.W. Ohse, ed, Blackwell

- Scientific Publications, Oxford, 1985, pp. 316-317.
- [17] Y. Waseda *The Structure of Non-Crystalline Materials*, McGraw-Hill, New York, 1980.
 - [18] W.G. Hoover, A.J.C. Ladd, and B. Moran, *Phys. Rev. Lett.* **48**, 1818 (1982); W.G. Hoover, *Molecular Dynamics*, Springer-Verlag, Berlin, 1986.
 - [19] B. Bernu, *Physica* **122A**, 129 (1983).
 - [20] K. Asai, K. Higuchi, M. Akimoto, H. Matsumoto and Y. Seo, “JAERI Monte Carlo Machine”, in *proceedings of the Joint International Conference on Mathematical Methods and Supercomputing in Nuclear Applications*, H. Künster, E. Stein and W. Werner, eds, Kernforschungszentrum, Karlsruhe, 1993, pp. 341.
 - [21] K.C. Ng, *J. Chem. Phys.* **61**, 2680 (1974).
 - [22] D.J.W. Geldart and S.H. Vosko, *Can. J. Phys.* **44**, 2137 (1966).
 - [23] O. Gunnarsson and B.I. Lundqvist, *Phys. Rev. B* **13**, 4274 (1976).
 - [24] U. Balucani, A. Torcini and R. Vallauri, *Phys. Rev. A* **46**, 2159 (1992).
 - [25] L. Dagens, M. Rasolt and R. Taylor, *Phys. Rev. B* **11**, 2726 (1982).
 - [26] S. Ranganathan, K. Pathak and Y. P. Varshni, *Phys. Rev. E* **49**, 2835 (1994).
 - [27] L. Reatto, D. Levesque and J. J. Weis, *Phys. Rev. A* **33**, 3451 (1986).

TABLES

TABLE I. Parameters used in the present QHNC-MD simulations for liquid alkali metals. $a = (4\pi n_0^{\text{I}}/3)^{-1/3}$ is the ion-sphere radius; $\Gamma = \beta e^2/a$ and $r_s = (4\pi n_0^{\text{e}}/3)^{-1/3}$ are the plasma parameter and the electron-sphere radius in units of the Bohr radius a_{B} , respectively. R_{c1} and R_{c2} are the cutoff length of the effective ion-ion potential $v_{\text{eff}}(r)$ in the MD simulation for the first MD run and second MD run [see text], respectively.

element	T (K)	Γ	r_s	Δt (fs)	R_{c1} (a)	R_{c2} (a)
Li	470	203.1	3.308	0.940	5.88	5.88
Na	373	209.1	4.046	2.349	7.06	7.06
K	338	185.9	5.024	3.996	6.76	6.76
Rb	313	187.2	5.388	6.585	6.81	6.80
Cs	303	180.3	5.781	8.954	6.83	6.84

FIGURES

FIG. 1. Flow chart of the QHNC-MD method. The initial potential $v_{\text{eff}}(r)$ is determined by approximating $g_{\text{II}}(r)$ in Equation (21) by the step function $\theta(r - a)$ with the ion-sphere radius a .

FIG. 2. The consistency measure $\Delta g_i(r)$ defined by Eq. 26) for liquid Li; dot-dashed curve, $\Delta g_1(r)$; dashed curve, $\Delta g_2(r)$. Solid curve is the final result for the ion-ion RDF $g_{\text{II}}(r)$.

FIG. 3. Comparison of the raw MD RDF for liquid Li with the extended RDF: dashed curve is the raw RDF data; solid curve is the extended RDF with the full potential by Eq. (20) with $B_{\text{MD}}(r)$; \circ is the result from the VMHNC equation for the present self-consistent potential. L is the side length of the simulation cell; $L/2 = 12.794a = 22.40\text{\AA}$ in the MD simulation for liquid Li with 4,000 particles. The discrepancy between the raw data and extended data becomes clear for $r \gtrsim 4a$, i.e., after the second peak of RDF. On the other hand, the extended RDF becomes identical to that of the VMHNC equation for $r \gtrsim 5a$, i.e., after the third peak of RDF.

FIG. 4. The ion-ion static structure factor $S_{\text{II}}(Q)$ for liquid Li: solid curve, the QHNC-MD result; dotted curve, result of the final step of the preparation phase (the QHNC-VM result); \circ , experimental result taken from [12]. The deviation of the VMHNC result from the experiment is corrected by the QHNC-MD method.

FIG. 5. The ion-ion static structure factors $S_{\text{II}}(Q)$ for liquid Na (the upper) and K (the lower): solid curve, the QHNC-MD result; dotted curve, the QHNC-VM result; \circ and \bullet , the neutron and X-ray experiments taken from [13] and [14], respectively.

FIG. 6. The ion-ion static structure factors $S_{\text{II}}(Q)$ for liquid Rb (the upper) and Cs (the lower): solid curve, the QHNC-MD result; dotted curve, the QHNC-MD result (the final step of the preparation phase); \circ and \bullet , the X-ray and neutron experimental results for Rb taken from [17] and [15], respectively. Experiment result for Cs denoted by \circ is taken from [13].

FIG. 7. The ion-ion radial distribution function $g_{II}(r)$ for liquid Na: solid curve, the QHNC-MD result; dotted curve, the QHNC-VM result; •, experimental result taken from [27]. The VMHNC approximation brings about small errors in the amplitude and phase compared with the experimental RDF.

FIG. 8. The electron-ion and ion-ion radial distribution functions for liquid Rb: solid curve, the QHNC-MD result; dotted curves, the QHNC-VM result; •, The electron-ion RDF derived by the use of the Ashcroft model potential. The electron-ion RDF has an inverse phase to the ion-ion RDF in their oscillation around unity.

FIG. 9. The electron charge distribution of a pseudoatom in liquid Rb: solid curve, the QHNC-MD result; dashed curve, the charge distribution of the 5s-electrons in a free Rb atom; •, The pseudopotential result with use of the Ashcroft model potential.

FIG. 10. The electron-ion RDF's for liquid alkali metals: inner-core structures near the origin are omitted.

FIG. 11. Effective ion-ion potentials for liquid alkali metals: Scaling properties are not found in the alkali potentials.

FIG. 12. The ion-ion RDF's for liquid alkali metals: The RDF's of Li, Na, K and Rb are written almost in a single curve in the units of length a , the ion-sphere radius. The RDF of Cs (the dotted curve) shows a small deviation; the dashed curve: Li. The difference among the results for Na, K, Rb are indiscernible on this scale.

Figure 1, Shaw Kambayashi and Junzo Chihara, Phys. Rev. E

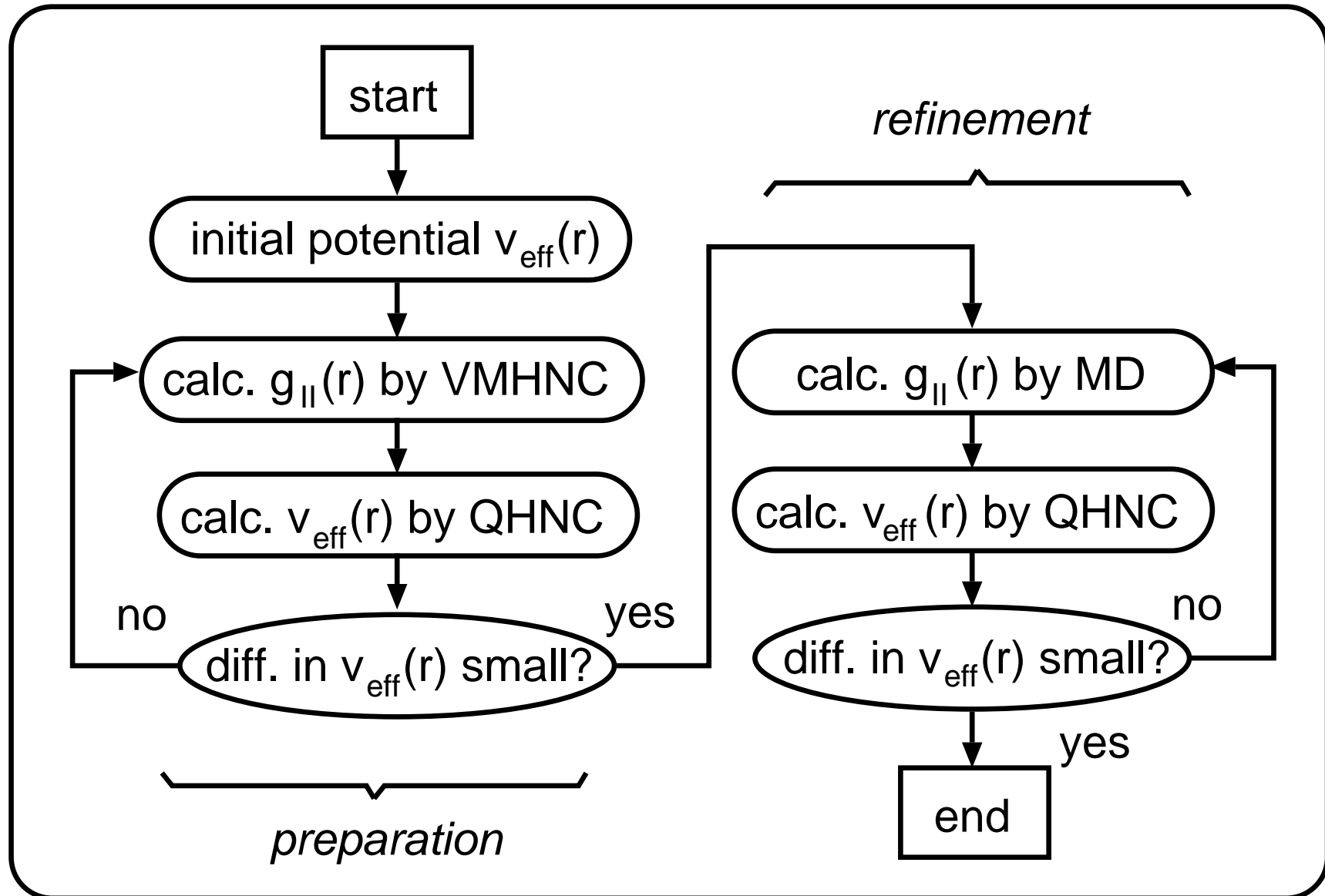


Figure 2, Shaw Kambayashi and Junzo Chihara, Phys. Rev. E

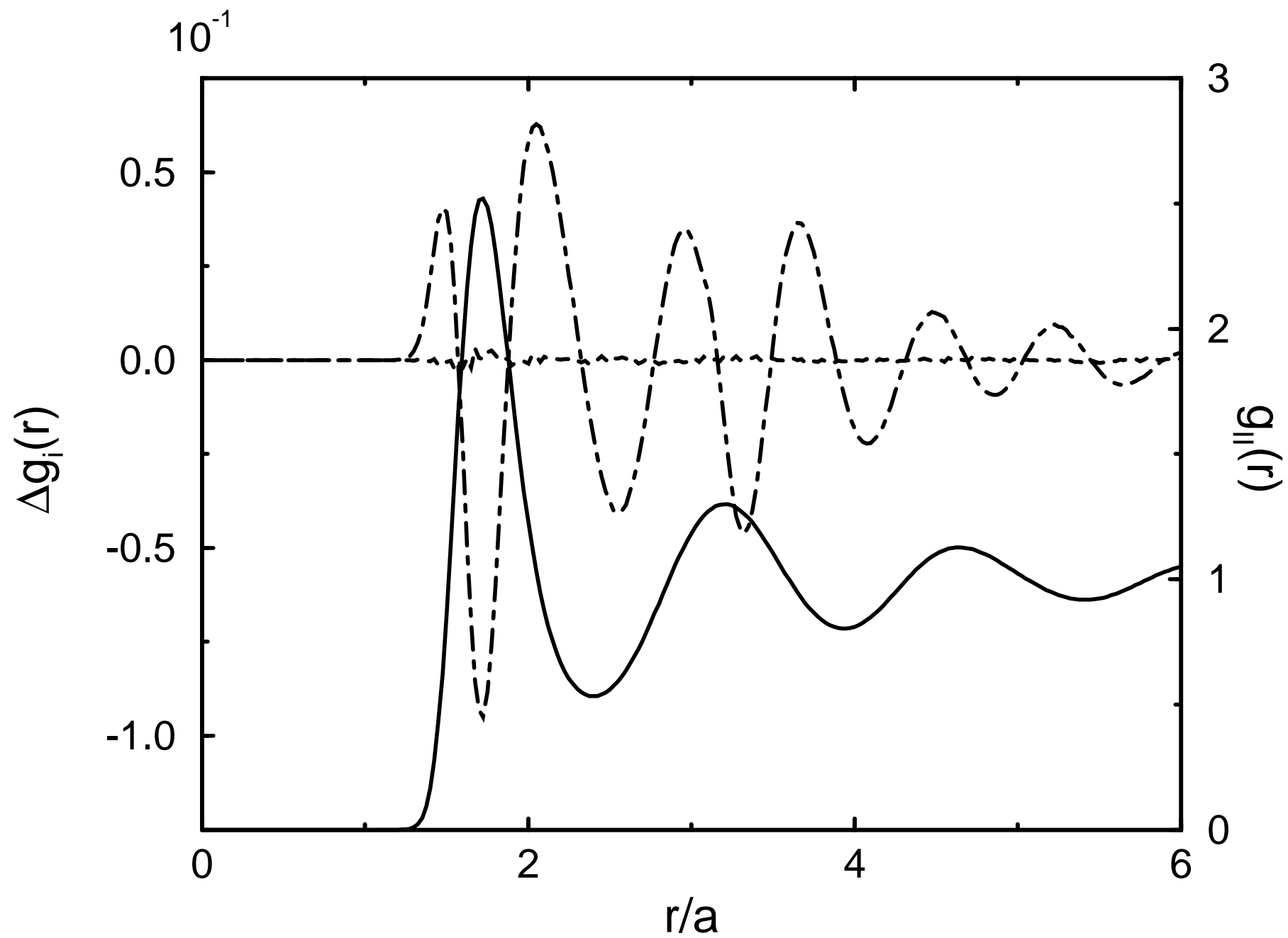


Figure 3, Shaw Kambayashi and Junzo Chihara, Phys. Rev. E

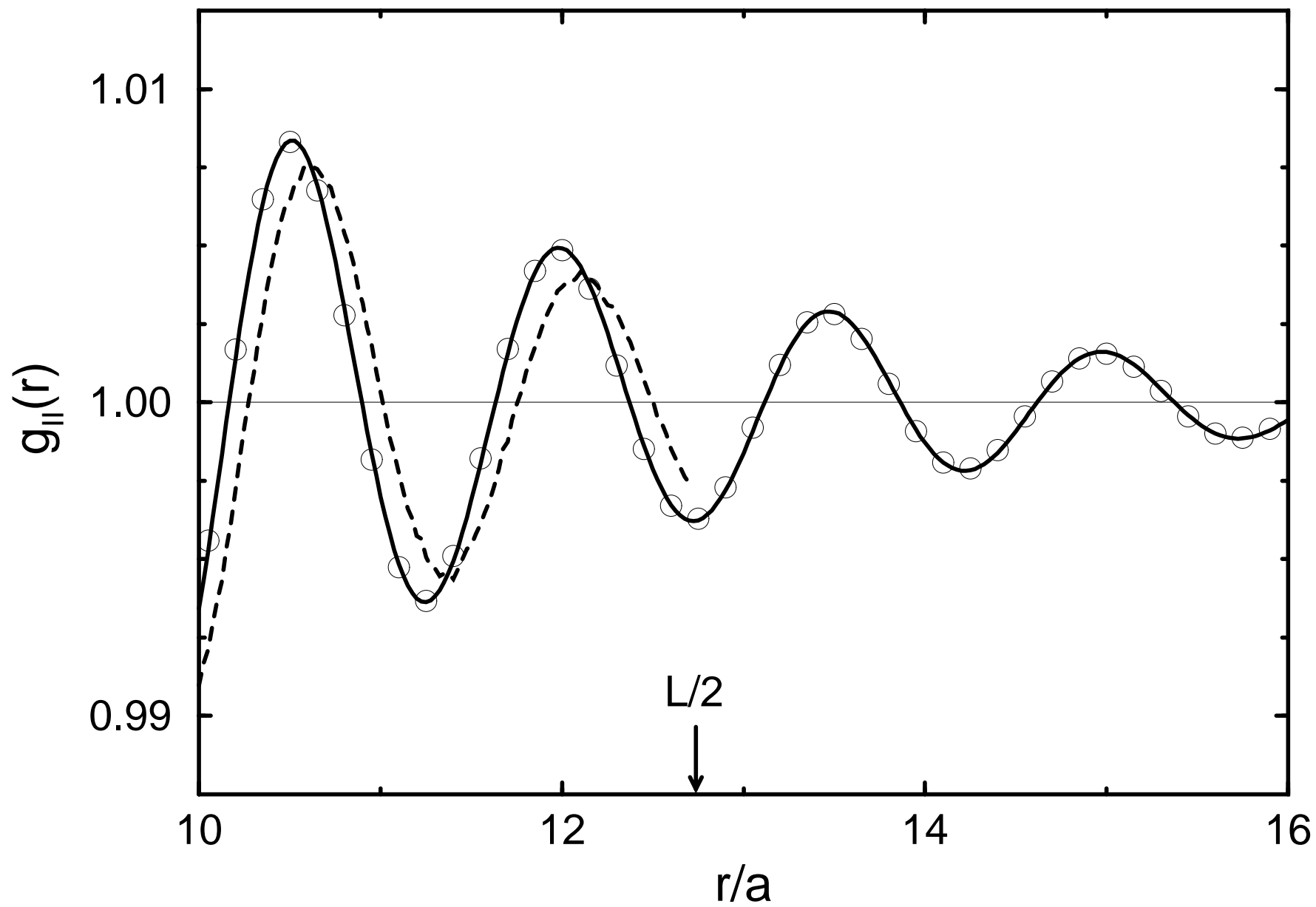


Fig. 4, Shaw Kambayashi and Junzo Chihara, Phys. Rev. E.

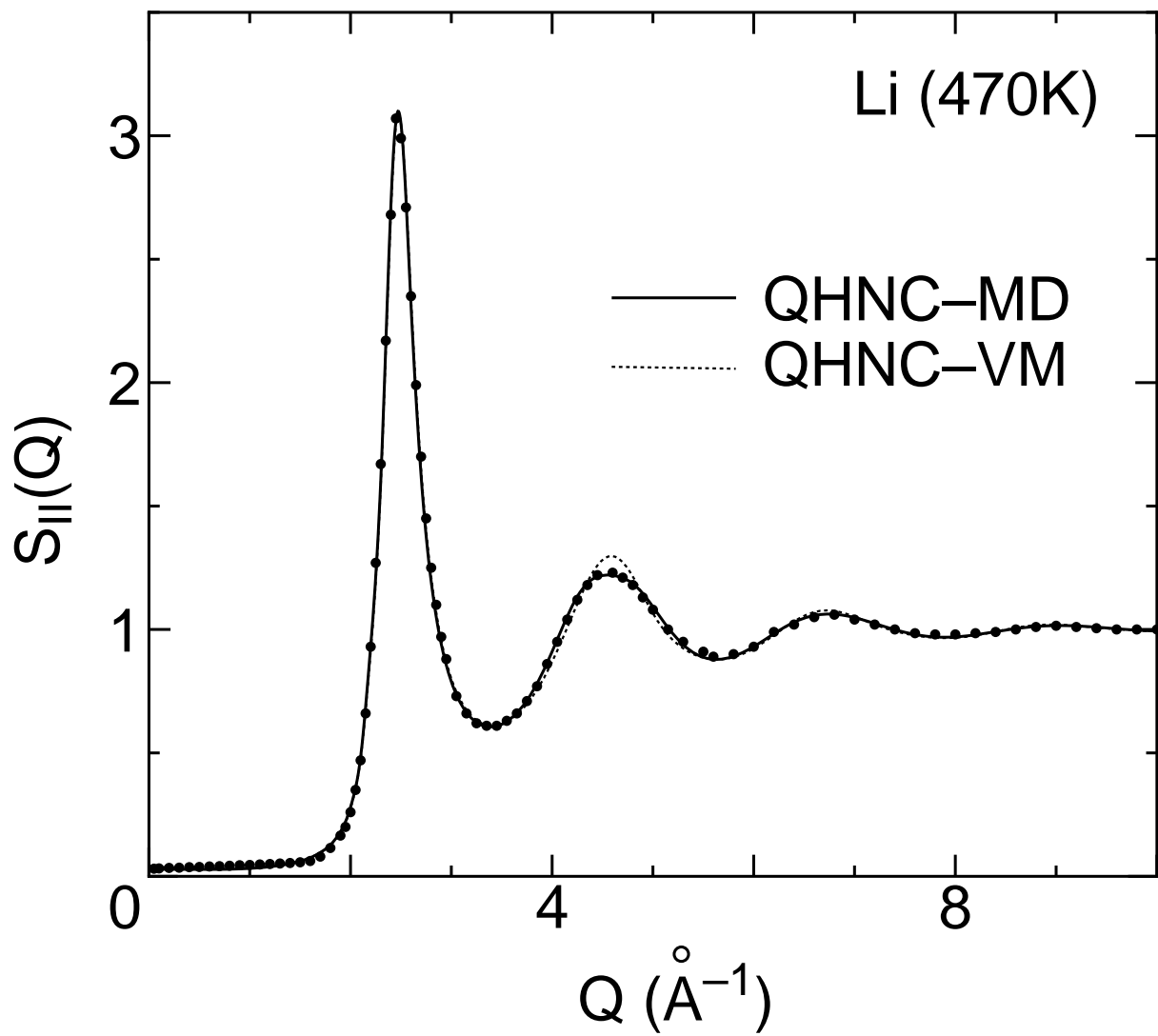


Fig. 5, Shaw Kambayashi and Junzo Chihara, Phys. Rev. E.

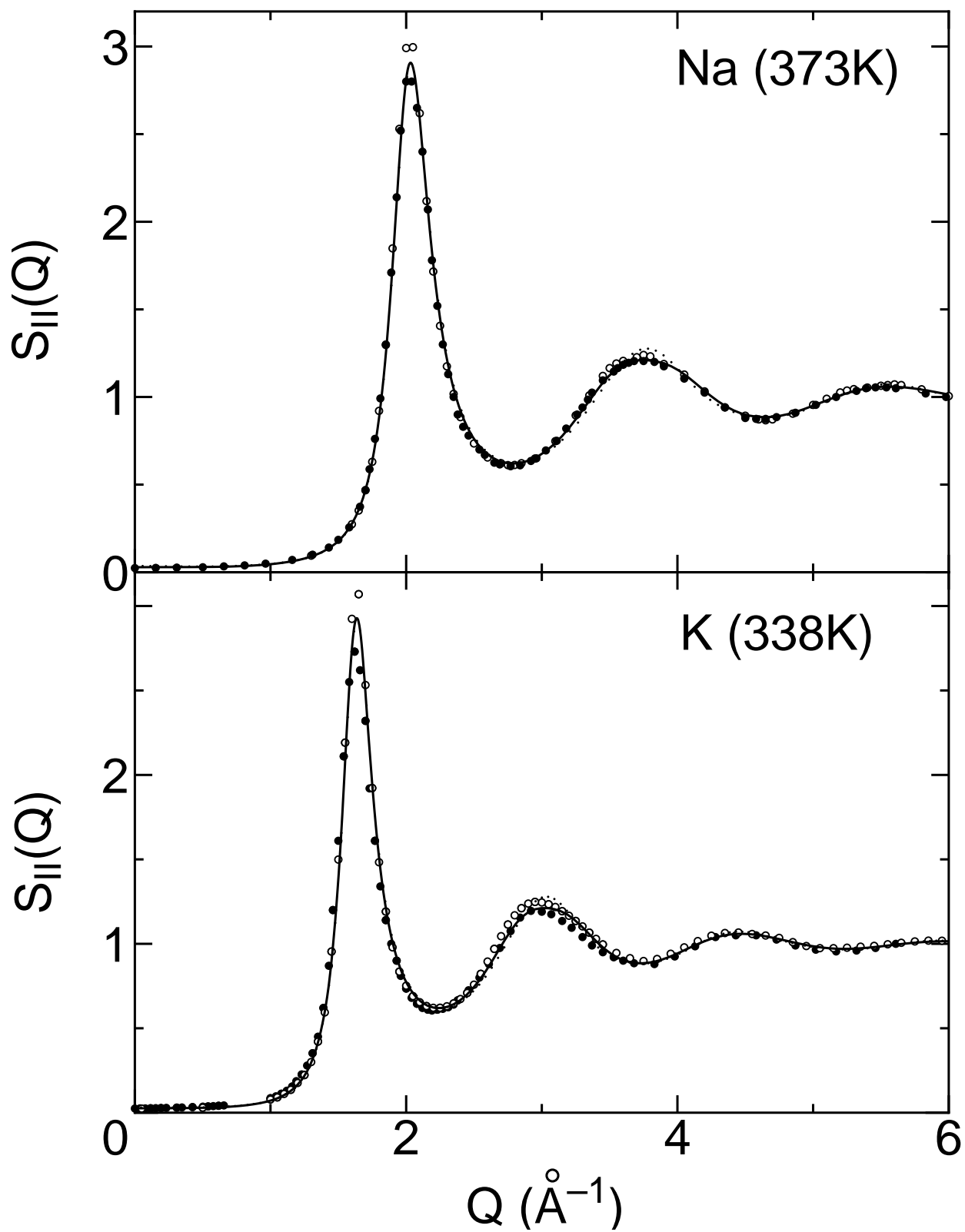


Fig. 6, Shaw Kambayashi and Junzo Chihara, Phys. Rev. E.

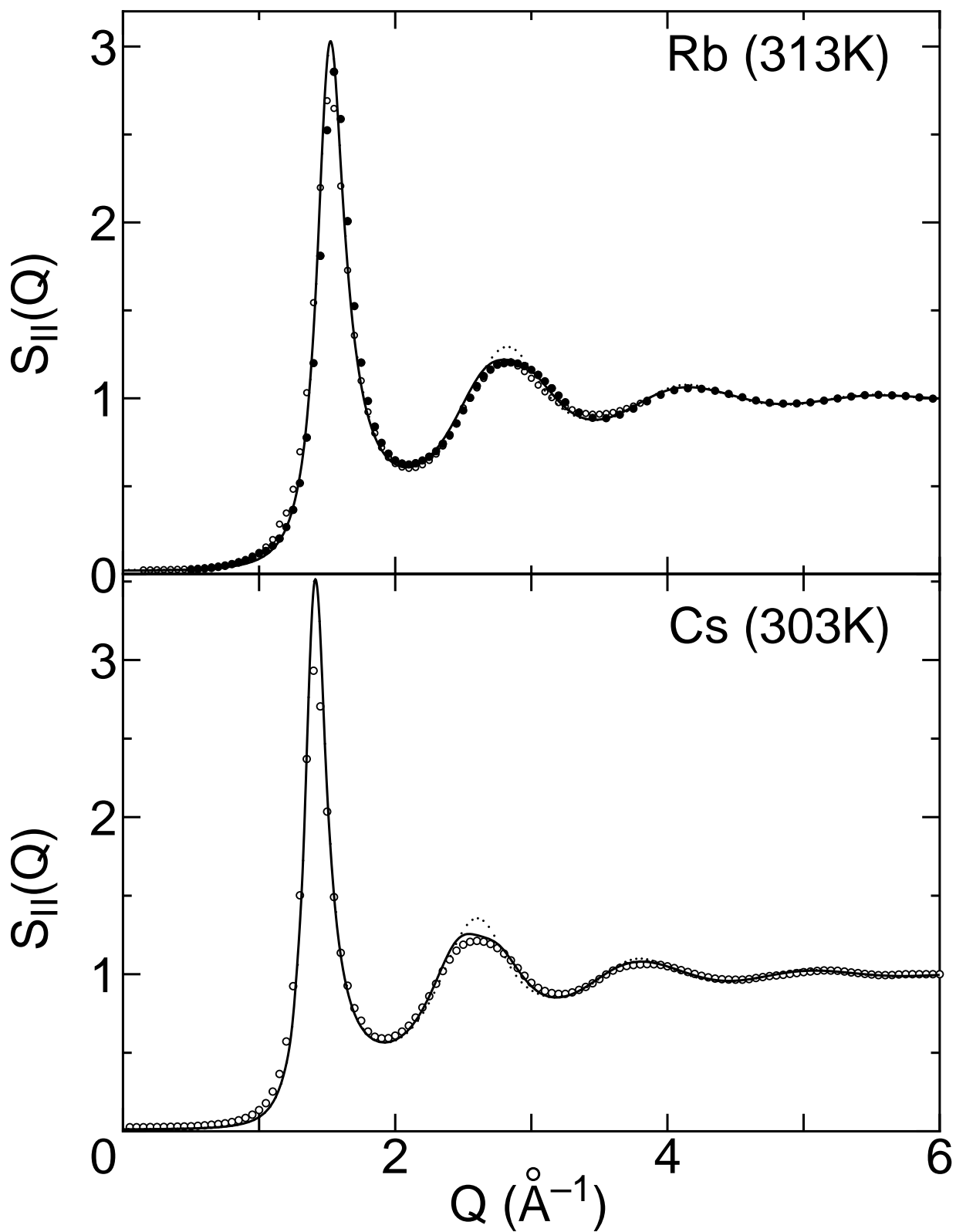


Fig. 7, Shaw Kambayashi and Junzo Chihara, Phys. Rev. E.

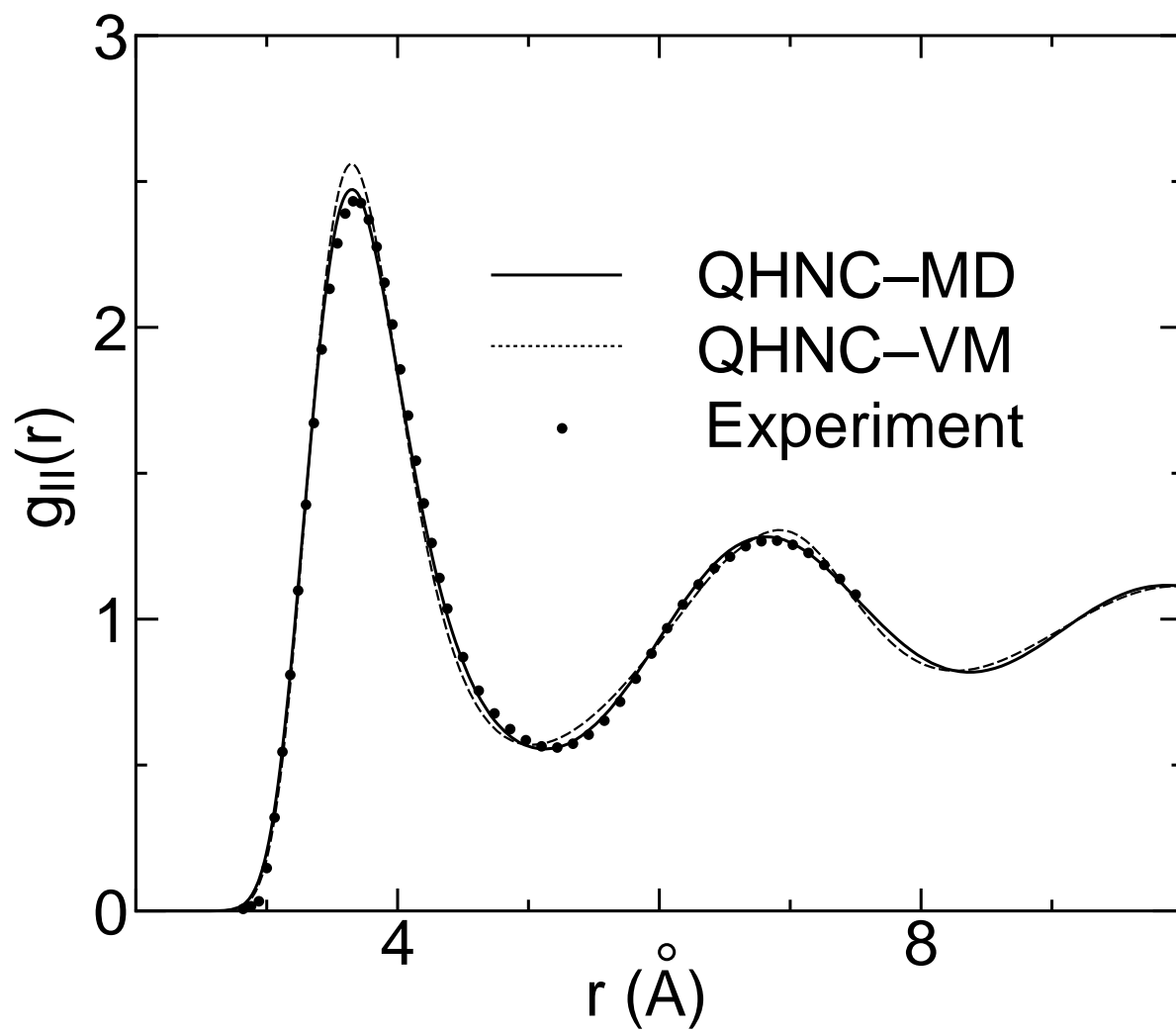


Fig. 8, Shaw Kambayashi and Junzo Chihara, Phys. Rev. E.

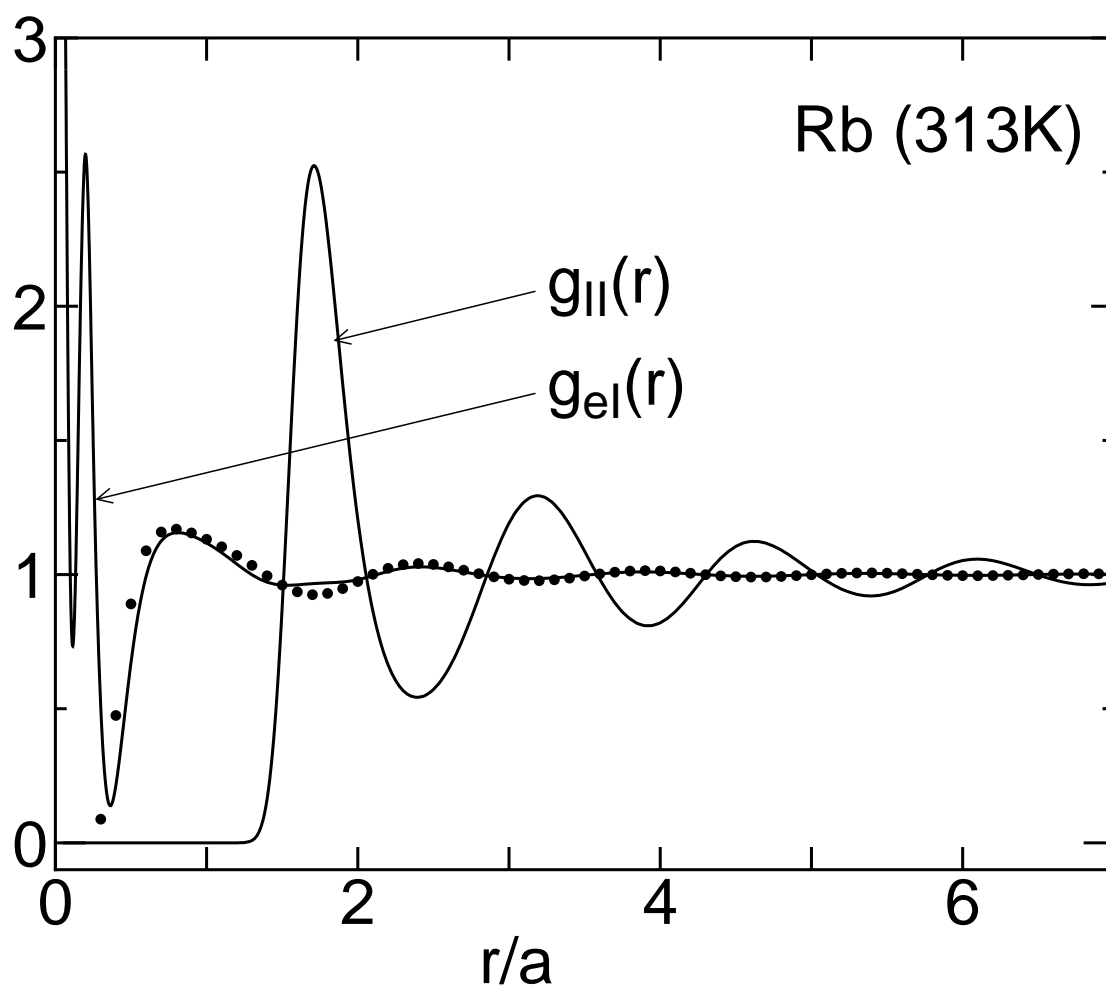


Fig. 9, Shaw Kambayashi and Junzo Chihara, Phys. Rev. E.

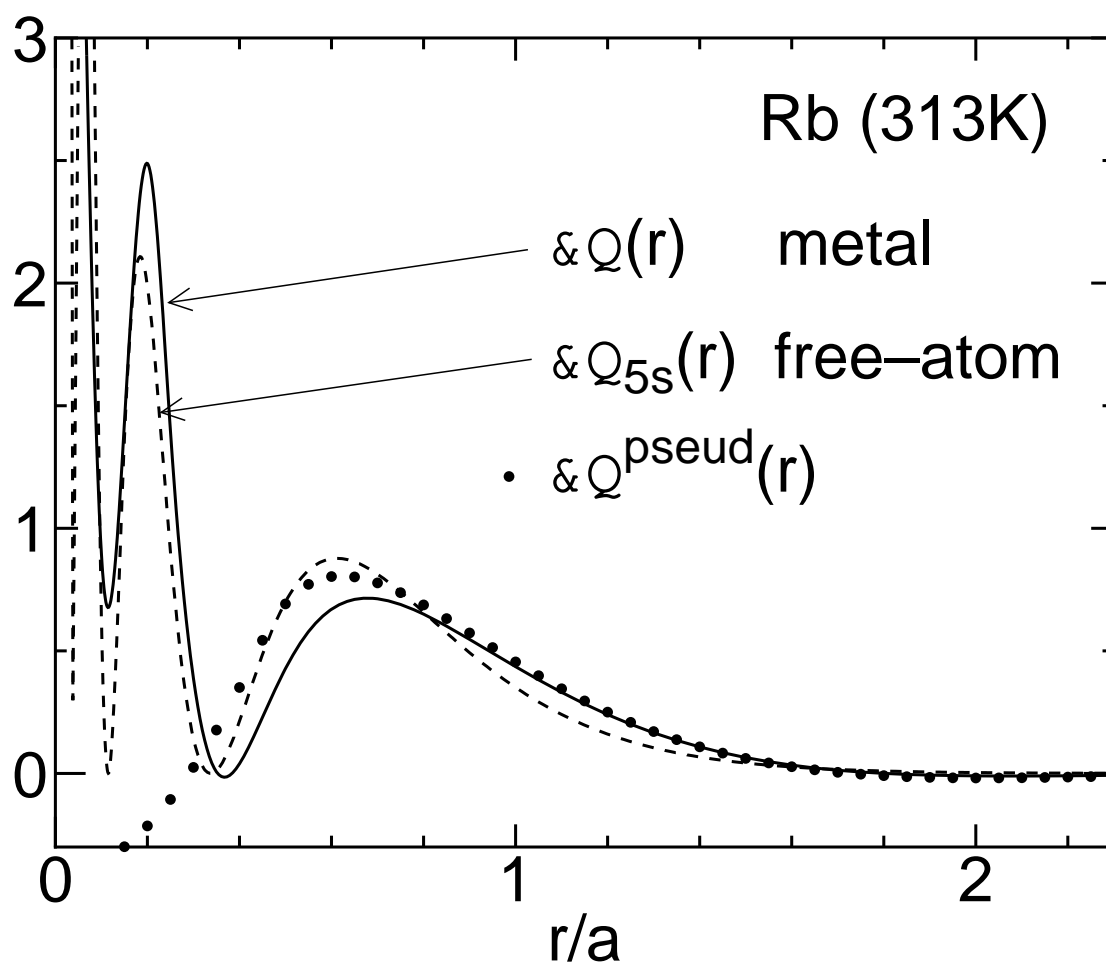


Fig. 10, Shaw Kambayashi and Junzo Chihara, Phys. Rev. E.

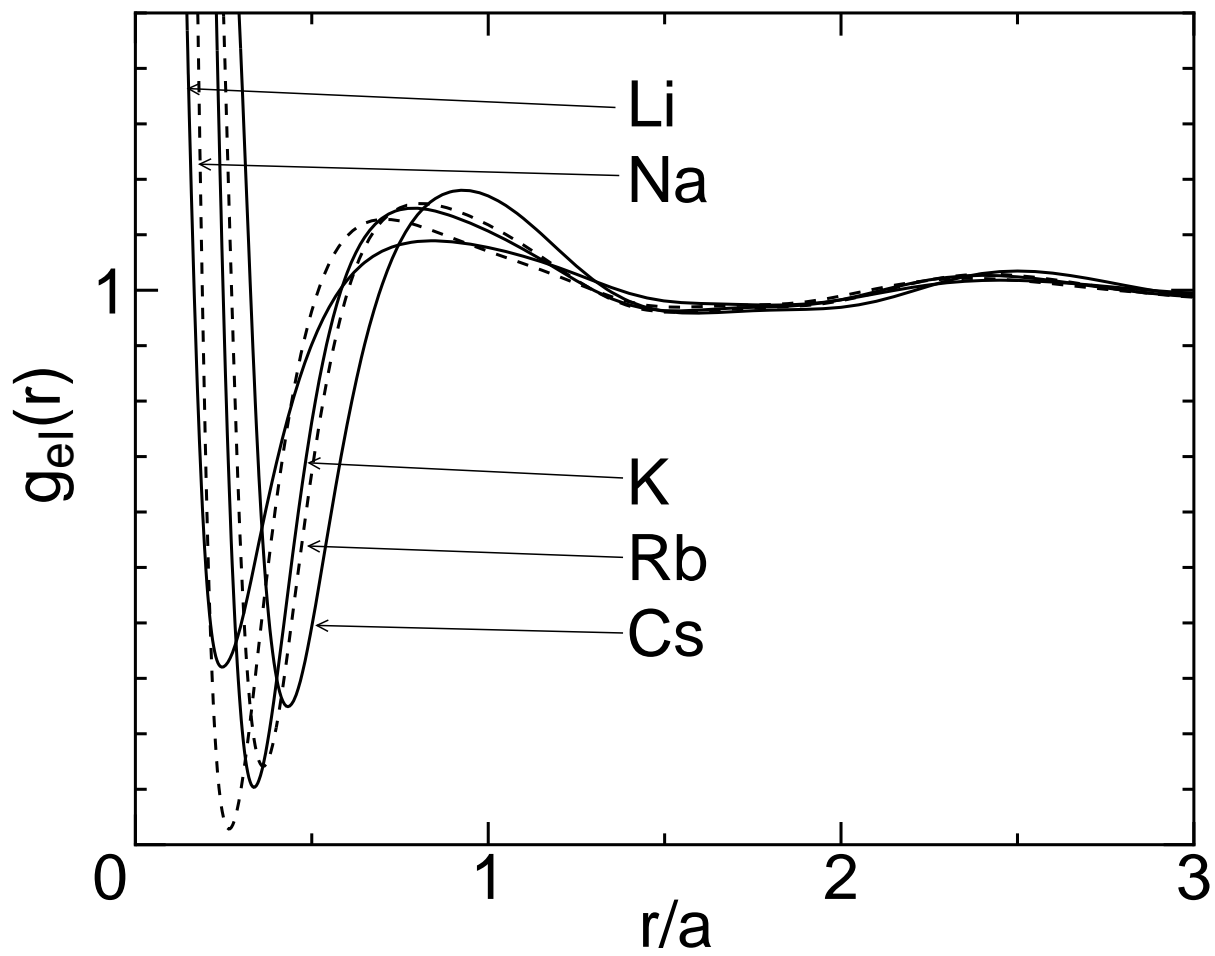


Fig. 11, Shaw Kambayashi and Junzo Chihara, Phys. Rev. E.

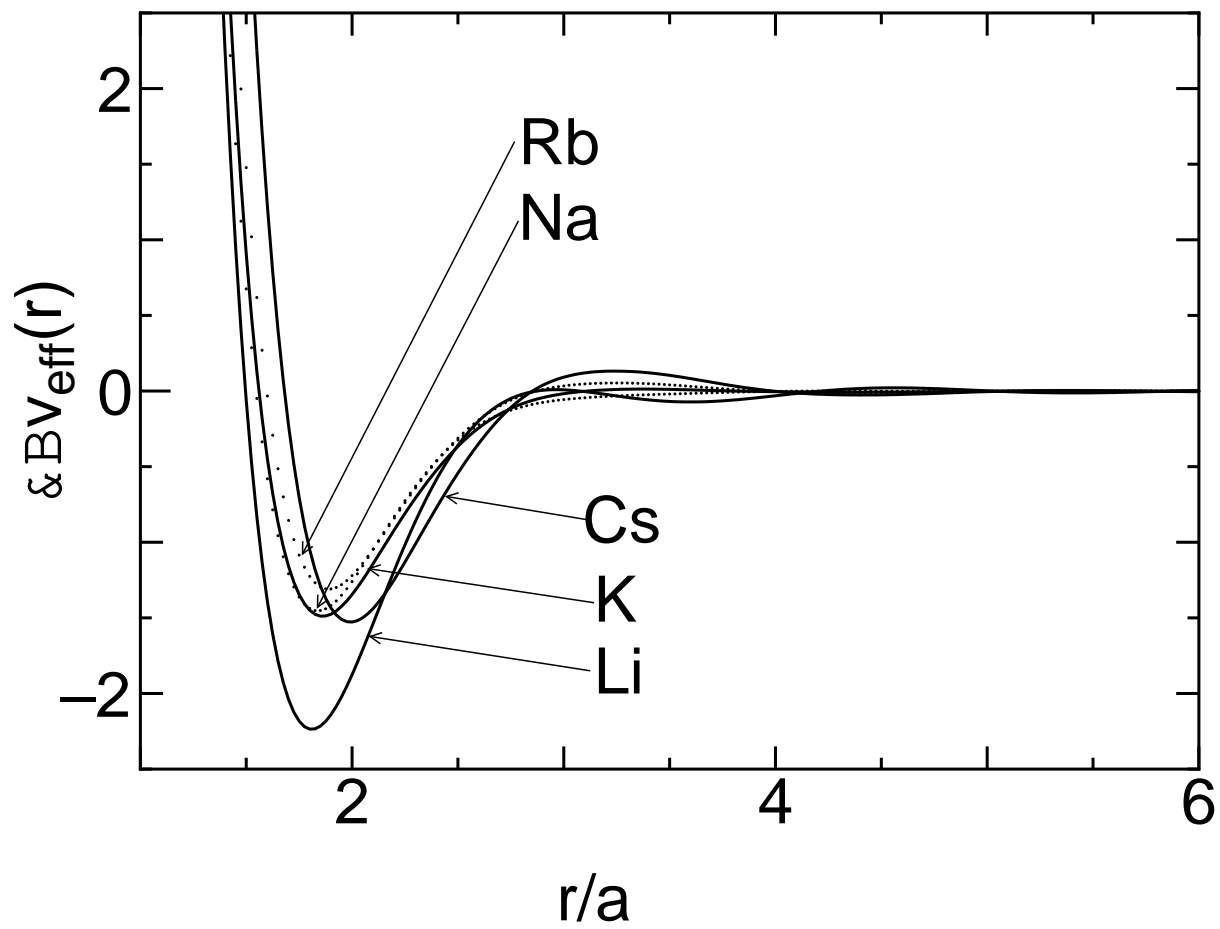


Fig. 12, Shaw Kambayashi and Junzo Chihara, Phys. Rev. E.

